Environ. Sci. Technol. **2003**, *37,* 616−623

Interpreting Deposition Patterns of Microbial Particles in Laboratory-Scale Column Experiments

NATHALIE TUFENKJI, JEREMY A. REDMAN, AND MENACHEM ELIMELECH*

Department of Chemical Engineering, Environmental Engineering Program, P.O. Box 208286, Yale University, New Haven, Connecticut 06520-8286

The transport and fate of microbial particles in subsurface environments is controlled by their capture (natural filtration) by sediment grains. Typically, filtration models used to describe microbe removal in porous media predict exponential decrease in microbial particle concentration with travel distance. However, a growing body of laboratory-scale column experiments suggests that the retained microbial particle profiles decay nonexponentially. The observed behavior may be attributed to the heterogeneity in the interactions between microbial particles and sediment grains, most likely due to the inherent variability in the microbial particles. This factor can be incorporated into classical colloid filtration (deposition) theory by inclusion of a distribution in the deposition rate coefficient. We show that certain distributions of the deposition rate coefficient (i.e., log-normal, bimodal, and power-law distributions) give rise to nonexponential deposition patterns. Comparisons of model predictions to experimental data indicate that the observed nonexponential deposition behavior of bacteria and virus particles may be attributed to a broad range (i.e., a power-law distribution) of microbial deposition rates. Other mechanisms such as particle release and blocking by previously deposited microbial particles are also shown to be potential sources of deviation from the classical filtration theory. Our results further suggest that monitoring fluid-phase particle concentration is insufficient for accurate characterization of the deposition and transport behavior of microbial particles in saturated porous media. Rather, the shape of the microbial particle retention profile is shown to be a key indicator of the mechanisms controlling microbial deposition and transport.

Introduction

Understanding the factors governing the transport and fate of microorganisms in subsurface environments is important for a number of engineering applications, including in-situ bioremediation (*1*), riverbank filtration (*2*), and land disposal of treated wastewater effluents (*3*). In most cases, the objective is to achieve a target concentration or specified degree of removal of the microorganisms at a given distance. Physicochemical filtration (deposition) has been recognized as the dominant mechanism responsible for the removal of microbial particles from the pore fluid, and, consequently, a great deal of effort has gone into investigating the factors that influence microbial attachment to sediments (*4*−*6*).

The most commonly used model for describing filtration of colloidal particles was developed by Yao et al. (*7*). In this "clean-bed" filtration model, the removal of suspended particles is represented by first-order kinetics, resulting in concentrations of suspended and retained particles that decline exponentially with distance. This model has been applied to laboratory-scale experiments involving the filtration of bacteria (*8*), viruses (*5*), and protozoa (e.g., *Cryptosporidium parvum* oocysts) (*9*).

Despite widespread use in modeling and experimental efforts, recent evidence suggests that filtration of microbial particles may not be consistent with the classical colloid filtration model. Direct evidence for the nonexponential removal of microorganisms can be found by examining microbial deposition patterns in laboratory-scale columns of uniform collector grains. Typically, these experiments involve radiolabeling the microorganism, dissecting the packed bed after a pulse of particles has been applied, and analyzing each slice for the presence of the radiolabel. Utilizing this procedure, Camesano and Logan (*6*) examined the influence of pore fluid velocity and ionic strength on the deposition profiles of the bacterial species *Pseudomonas fluorescens* P17. In the majority of the column experiments presented, the deposition rates declined monotonically with distance. Using a packed bed of highly cleaned quartz grains, Redman et al. (*10, 11*) observed that the profile of retained viruses decayed according to a power-law. Several additional laboratory-scale column studies involving the measurement of deposited microorganism concentration (*12*−*15*) as well as those monitoring the fluid-phase concentration (*16*) further demonstrate that filtration of viruses and bacteria often deviates from the classical colloid filtration model.

Various explanations have been offered to account for this behavior, including heterogeneity in the microbial population (*14, 16*) and in the collector grain surface (*17*). One way to account for this variability is to incorporate a distribution of attachment efficiencies (or deposition rates) into the classical particle filtration (deposition) theory. Baygents et al. (*14*) found that monoclonal suspensions of two bacterial species exhibited bimodal distributions in electrophoretic mobility and that the nonexponential retained particle profiles were best modeled using a bimodal distribution of the attachment efficiency. In a theoretical investigation, Bolster et al. (*18*) showed that a bimodal distribution in bacterial attachment efficiency may go unnoticed when relatively short packed columns are considered, but it becomes apparent and results in nonexponential deposition behavior when longer travel distances are considered. This behavior was demonstrated in their column experiments with the Gram-negative bacterial strain designated W31 where nonexponential microbial deposition profiles were observed only in experiments where longer columns were used (*13*).

In this paper, we systematically analyze the factors controlling the shape of the retained and fluid-phase microbial particle concentration profiles in packed columns. We show that certain asymmetric distributions of the deposition rate coefficient, which reflect the inherent heterogeneity of the microbial particles, give rise to nonexponential deposition patterns. We also identify two other potential sources of deviation from classical colloid filtration theory, namely microbial deposition dynamics (blocking)

* Corresponding author phone: (203)432-2789; fax: (203)432-2881; e-mail: menachem.elimelech@yale.edu.

10.1021/es025871i CCC: $25.00
Published on Web 01/04/2003

and release of microbial particles from collector grains. The results suggest that observing fluid-phase particle concentration may not be sufficient for complete description of microbial deposition and transport behavior in saturated porous media. To identify the dominant mechanisms controlling microbial deposition and transport in porous media, it is imperative that the concentration profile of retained microbial particles be determined in conjunction with the particle breakthrough curve.

Colloid Filtration Theory and Microbial Deposition Patterns

Microbial Particle Transport and Deposition Equation. The transport of colloidal particles, including microorganisms such as bacteria and viruses, through saturated homogeneous porous media can be described by accounting for particle advection, hydrodynamic dispersion, and deposition (filtration). Because residence times in laboratory-scale column experiments are usually short, inactivation of microorganisms is negligible. Additionally, for relatively low particle concentration and moderate ionic strength, blocking and ripening effects are not important, and particle release is typically negligible. Under these conditions, the concentrations of suspended particles $C(x,t)$ and deposited particles $S(x,t)$ at a column depth x and time t can be modeled by a one-dimensional advection-dispersion equation with a term for first-order particle deposition kinetics (*19*, *20*):

$$\frac{\partial C}{\partial t} + \frac{\rho_b}{\epsilon}\frac{\partial S}{\partial t} = D\frac{\partial^2 C}{\partial x^2} - v\frac{\partial C}{\partial x} \tag{1}$$

$$\frac{\rho_b}{\epsilon}\frac{\partial S}{\partial t} = kC \tag{2}$$

Here, v is the interstitial particle velocity, D is the hydrodynamic dispersion coefficient, ϵ is the bed porosity, ρ_b is the porous medium bulk density, and k is the particle deposition rate coefficient. The latter is related to the commonly used single collector efficiency η via (*7*)

$$k = \frac{3(1-\epsilon)v}{2d_c}\eta \tag{3}$$

where d_c is the diameter of the collector grains. Note that in colloid and microbial transport/filtration studies, the single collector efficiency (determined experimentally) is commonly expressed as $\eta = \alpha\eta_0$, with α being the collision (attachment) efficiency and η_0 the single collector efficiency for favorable deposition (usually calculated from filtration theory) (*7*).

Classical Analytical Solutions for Microbial Deposition Patterns. Colloid filtration theory has been used extensively in modeling the transport of microorganisms such as bacteria and viruses in saturated porous media (*10*, *12*, *21*, *22*). In this transport modeling, it is typically assumed that the rate of particle deposition is both spatially and temporally invariant, i.e., a single value of k is specified. In this section, we present solutions to eqs 1 and 2 for several degrees of complexity and later use the derived equations to determine the concentration profiles of retained and suspended particles as a function of travel distance.

Steady-State Filtration with No Dispersion. For steady-state filtration and negligible hydrodynamic dispersion effects, eqs 1 and 2 are reduced to

$$v\frac{dC}{dx} + kC = 0 \tag{4}$$

Applying the inlet boundary condition $C = C_0$ at $x = 0$, the solution to eq 4 is straightforward. For a continuous particle injection at concentration C_0 and a time period t_0, the solutions for a column initially free of deposited particles read

$$C(x) = C_0\exp\left[-\frac{k}{v}x\right] \tag{5}$$

$$S(x) = \frac{t_0\epsilon k}{\rho_b}C(x) = \frac{t_0\epsilon k C_0}{\rho_b}\exp\left[-\frac{k}{v}x\right] \tag{6}$$

This classical form of the filtration equation was first suggested by Iwasaki (*23*) based on experimental observations of sand filtration. The ratio k/v in the above equations is equivalent to the filter coefficient λ introduced by Iwasaki.

Complete Steady-State Solution. When dispersion effects are considered, a second boundary condition at the column outlet ($x = L$) is specified:

$$\left.\frac{dC}{dx}\right|_{x=L} = 0 \tag{7}$$

The steady-state solutions of eqs 1, 2, and 7 for the spatial distribution of suspended and retained particles are respectively (*24*)

$$C(x) = C_0 \times \left\{\frac{\exp\left[\frac{vx}{2D}(1-\omega)\right] + \frac{(\omega-1)}{(\omega+1)}\exp\left[\frac{vx}{2D}(1+\omega) - \frac{vL\omega}{D}\right]}{1 + \frac{(\omega-1)}{(\omega+1)}\exp\left[-\frac{vL\omega}{D}\right]}\right\} \tag{8}$$

$$S(x) = \frac{t_0\epsilon k}{\rho_b}C(x) \tag{9}$$

where

$$\omega = \sqrt{1 + \frac{4kD}{v^2}} \tag{10}$$

Complete Unsteady-State Solution. To study the influence of filtration time on particle deposition patterns, the governing equations can be solved using the Laplace transform technique subject to the following initial and boundary conditions (*24*−*26*):

$$C(x,0) = 0 \tag{11a}$$

$$C(0,t) = \begin{cases} C_0 & 0 < t \le t_0 \\ 0 & t > t_0 \end{cases} \tag{11b}$$

$$\frac{\partial C}{\partial x}(\infty,t) = 0 \tag{11c}$$

The analytical solutions to eqs 1, 2, and 11 are

$$C(x,t) = \begin{cases} C_1(x,t) & 0 < t \le t_0 \\ C_1(x,t) - C_1(x,t-t_0) & t > t_0 \end{cases} \tag{12}$$

where

$$C_1(x,t) = \frac{C_0}{2}\left\{\exp\left[\frac{(v-v\omega)x}{2D}\right]erfc\left[\frac{x - v\omega t}{2\sqrt{Dt}}\right] + \exp\left[\frac{(v+v\omega)x}{2D}\right]erfc\left[\frac{x + v\omega t}{2\sqrt{Dt}}\right]\right\} \tag{13}$$

and

$$S(x,t) = \frac{\epsilon}{\rho_b} k \int_0^t C(x,t)\, dt \qquad (14)$$

where $C(x,t)$ is given by eq 12.

Comparison of Predicted Microbial Deposition Patterns. Particle concentration profiles (presented in a semilog format) predicted by the analytical solutions to eqs 1 and 2 for the three different cases discussed above are compared in Figure 1. The parameters used in the calculations (Table 1) are representative of column studies involving microbial particles. The classical clean-bed filtration model (case a, eqs 5 and 6) predicts an exponential decline in suspended and retained particle concentration with distance (Figure 1a,b, respectively). As shown in the figure, the inclusion of hydrodynamic dispersion effects (case b, eqs 8−10) and a discontinuous step injection of influent particles (case c, eqs 12−14) do not noticeably influence the particle filtration behavior. The results indicate that (i) both the suspended and deposited particle concentrations decline exponentially with distance and (ii) the classical filtration model, which is a solution to the simplified form of eqs 1 and 2, adequately captures the particle deposition behavior in typical (advection-dominated), one-dimensional column experiments.

Deviations from Classical Colloid Filtration Theory. Although colloid filtration theory predicts an exponential decline in suspended and retained particle concentrations with distance, numerous laboratory studies have shown that the profiles of retained microbial particles decay in a nonexponential fashion (*6*, *10*−*16*). Table 2 summarizes studies involving microbial particles where a clear nonexponential deposition behavior is observed. The causes for such nonexponential deposition behavior are analyzed and discussed in the following subsections.

Heterogeneity in the Microbial Deposition Rate Coefficient. The expectation of an exponentially decaying particle concentration profile is based on the assumption of a constant deposition rate coefficient, k, or single-collector efficiency, η, and thus a constant value for the attachment efficiency, α. Discrepancies between predicted and observed microbial deposition patterns may result from a distribution in deposition rates caused by variability in the microbial particle-collector grain interactions. Local variations in the surface chemistry or charge on the microbes, distribution in the microbe average surface (ζ) potential, and polydispersivity in the microbe size give rise to heterogeneity in the microbial particles and the resulting deposition rate coefficient (*27*−*29*).

These heterogeneity effects can be incorporated into classical colloid filtration theory by inclusion of a distributed deposition rate coefficient, k. Here, we consider the classical clean-bed filtration model (eqs 5 and 6) and incorporate various probability distribution functions $p(k)$ of the deposition rate coefficient to determine the suspended and deposited particle concentration profiles:

$$C(x) = C_0 \int_0^\infty \exp\left[-\frac{k}{v}x\right] p(k)\, dk \qquad (15)$$

$$S(x) = \frac{\epsilon t_0 C_0}{\rho_b} \int_0^\infty k \exp\left[-\frac{k}{v}x\right] p(k)\, dk \qquad (16)$$

(a) Normal Distribution. First, we assume a normal (Gaussian) distribution in k

$$p(k) = \frac{1}{\sigma\sqrt{2\pi}} \exp\left[-\frac{1}{2}\left(\frac{k-\bar{k}}{\sigma}\right)^2\right] \qquad (17)$$

where $\bar{k}$ is the mean deposition rate coefficient and σ is the standard deviation.

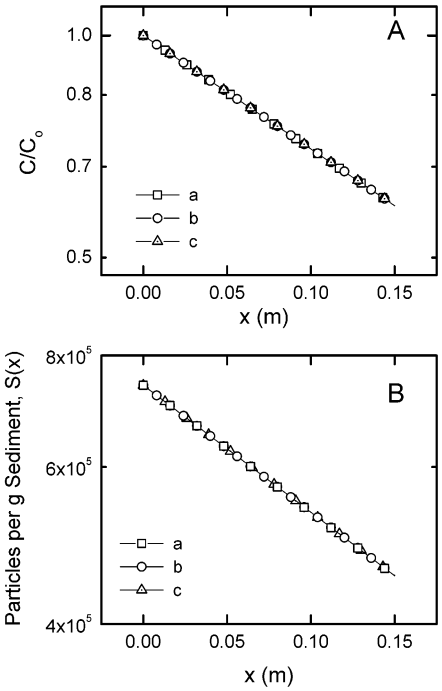

FIGURE 1. Comparison of (A) normalized suspended particle concentration profiles and (B) retained particle concentration (number of deposited particles per gram of collector grains) as a function of distance *x* for three different cases: (a) steady-state analytical solution with no dispersion (eqs 5 and 6), (b) complete steady-state analytical solution (eqs 8−10), and (c) unsteady-state analytical solution (eqs 12−14). In the latter, *S*(*x*) is calculated at $t > t_0$, (i.e., at 2100 s) to account for deposition occurring during the transient, elution portion of the particle breakthrough curve. Note that data are presented in a semilog format. Parameters used in the calculations are summarized in Table 1.

(b) Log-Normal Distribution. The second probability distribution function considered is a log-normal distribution

$$p(k) = \frac{1}{k\tilde{\sigma}\sqrt{2\pi}} \exp\left[-\frac{1}{2}\left(\frac{\ln k - \tilde{k}}{\tilde{\sigma}}\right)^2\right] \qquad (18)$$

where $\tilde{k}$ and $\tilde{\sigma}$ are the mean and standard deviation of the log-normally distributed k, respectively (*30*). Note that $\tilde{k}$ is related to $\bar{k}$ of the normal distribution by $\tilde{k} = \ln \bar{k} - \tilde{\sigma}^2/2$ (*30*). The rationale behind the use of a log-normally distributed deposition rate coefficient is based on the Derjaguin-Landau-Verwey-Overbeek (DLVO) theory of colloid stability (*31*, *32*). When a particle comes into close proximity of a similarly charged collector grain, overlapping of the respective electrostatic double layers gives rise to a repulsive electrostatic energy barrier. The height of this barrier (Φ_{max}) is proportional to the product of the surface (or ζ) potentials of both the particle and collector grain and the size (radius) of the particle (*29*). In natural systems, the surface potentials of the microbial particle and sediment grains as well as the microbe size are random variables and are usually normally distributed. Since the deposition rate coefficient is related to the energy barrier by an Arrhenius-type relationship, $k \propto \exp(-\Phi_{max}/k_bT)$ (*33*) (k_bT is the product of Boltzmann's constant and absolute temperature), we expect k to be closely log-normally distributed.

(c) Bimodal Distribution. Several studies have proposed a discrete bimodal function to account for heterogeneous deposition in a microbial population, where it is assumed that the original population consists of two subpopulations with different attachment efficiencies, α (*13*, *14*, *16*, *18*). Here, we adopt a bimodal function consisting of two distinct normal

TABLE 1. Summary of Parameters Used in Calculation of Particle Concentration Profiles

parameter		parameter	
column length, L	15 cm	time length of injection, t_0	1500 s
particle radius, a_p	0.5 μm	bulk density, ρ_b	1.33 g/cm^3
collector (grain) radius, a_c	0.1 mm	influent particle concentration, C_0	1×10^6 cm^{-3}
bed porosity, ϵ	0.40	approach velocity,[c] u_0	2×10^{-4} m/s
longitudinal dispersivity,[a] α_L	5×10^{-4} m	collision efficiency, α	0.10
single-collector efficiency for favorable deposition,[b] η_0	7.3×10^{-3}	particle deposition rate coefficient,[d] k	1.64×10^{-3} s^{-1}

[a] The dispersion coefficient D is calculated as the product of the longitudinal dispersivity and interstitial velocity. [b] The following parameters are used in the calculation of η_0 based on filtration theory (*29*): Hamaker constant, 1×10^{-20} J; fluid density, 1.00 g/cm^3; particle density, 1.08 g/cm^3; fluid viscosity, 1.06×10^{-3} Pa/s; and temperature, 20 °C. [c] The approach velocity is equal to the product of interstitial velocity and porosity. [d] Calculated using eq 3, with $\eta = \alpha\eta_0$.

TABLE 2. Summary of Laboratory Column Studies with Microbial Particles Where Nonexponential Deposition Is Observed

source (ref)	microbial particle	sediment grain	column length (cm)	solution chemistry	observations on deposition pattern
(*6*)	*Pseudomonas fluorescens* P17 and *Burkholderia (Pseudomonas) cepacia* G4	Southern AZ soil	7	AGW,[a] IS 4×10^{-3} M	several experiments resulted in patterns which resemble a power law (i.e., straight line on a log−log plot, R^2 ranges from 0.83 to 0.99)
(*10*)	recombinant Norwalk virus	quartz sand	29	NaCl, pH 6.9, IS 10^{-2} M	strongly resembles a power law ($R^2 = 0.95$, 0.99)
(*12*)	motile, Gram-negative bacteria designated A1264	borosilicate glass	1, 2	MOPS[d] buffer, pH 7.7	strongly resembles a power law ($R^2 = 0.97$)
(*13*)	nonmotile Gram-negative bacteria designated W31	Oyster, VA sediment	15, 43, 45	AGW,[b] pH 6.2	nonexponential behavior is observed with longer columns
(*14*)	bacteria A1264 and nonmotile Gram-negative bacteria designated CD1	borosilicate glass	1	MOPS[d] buffer, pH 7.0, IS 10^{-2} M	strongly resembles a power law ($R^2 = 0.99$)
(*15*)	*Pseudomonas fluorescens* P17	quartz sand	1−10.5	(a) AGW,[c] pH 8.0, IS 3.6×10^{-3} M	(a) in low ionic strength (IS) solution, strongly resembles power law ($R^2 = 0.98$)
				(b) $CaCl_2$ solution, pH 6.8, IS 6×10^{-2} M	(b) in high IS solution, deposition pattern is exponential ($R^2 = 0.90$)

[a] Artificial groundwater (AGW) solution prepared as described by ref *41*. [b] Artificial groundwater (AGW) solution consists of (per liter of deionized water): 0.06 g $MgSO_4 \cdot 7H_2O$, 0.036 g $NaHCO_3$, 0.036 g $CaCl_2$, 0.035 g $Ca(NO_3)_2$, 0.025 g $CaSO_4 \cdot 2H_2O$, and 0.02 g KNO_3. [c] Artificial groundwater (AGW) solution consists of (per liter of deionized water): 0.069 g $MgSO_4 \cdot 7H_2O$, 0.050 g $NaHCO_3$, 0.00145 g $CaCl_2 \cdot 2H_2O$, 0.064 g $Ca(NO_3)_2 \cdot 4H_2O$, and 0.002 g KF. [d] 3-[*N*-morpholino]propanesulfonic buffer

distributions in order to account for the more realistic wider range of deposition rates, rather than limiting the choice to two discrete values

$$p(k) = f_{low} \frac{1}{\sigma_{low}\sqrt{2\pi}} \exp\left[-\frac{1}{2}\left(\frac{k - \bar{k}_{low}}{\sigma_{low}}\right)^2\right] + f_{high} \frac{1}{\sigma_{high}\sqrt{2\pi}} \exp\left[-\frac{1}{2}\left(\frac{k - \bar{k}_{high}}{\sigma_{high}}\right)^2\right] \quad (19)$$

where $\bar{k}_{low}$ and $\bar{k}_{high}$ are the mean deposition rate coefficients, σ_{low} and σ_{high} are the corresponding standard deviations, and f_{low} and f_{high} are the fractions of the total population associated with each mode.

(d) Power-Law Distribution. Redman et al. (*11*) propose a filtration model which assumes that heterogeneity leads to a power-law distribution of particle deposition rates. Thus, the last distribution function we consider here is the power-law distribution

$$p(k) = Ak^{-b} \quad (20)$$

where the premultiplier A and power-law exponent b are constants. Unlike the previous distributions, the power-law distribution is not a probability density function (*11*). Hence, the lower and upper limits of the integral in eqs 15 and 16 are set to a minimum (k_{min}) and maximum (k_{max}) deposition rate coefficient, respectively.

Comparison of Predicted Microbial Deposition Patterns. Concentration profiles of suspended and retained particles calculated using the above four different distribution functions are compared to those obtained using a constant deposition rate coefficient in Figure 2 (parts a and b, respectively). The parameters used in these calculations are summarized in Tables 1 and 3, with the exception that the column length has been extended to 50 cm and the time of injection, t_0, has been increased to 5000 s. As discussed previously, a constant k (1.64×10^{-3} s^{-1}) results in an exponential (or linear on a semilog plot) decay in suspended and retained particle concentration with distance (curve a). Curve b in Figure 2a,b was generated by incorporating a normally distributed k in the classical colloid filtration model, with $\bar{k} = 1.64 \times 10^{-3}$ s^{-1} and $\sigma = 0.25\bar{k}$. Although a normally distributed deposition rate coefficient implies heterogeneity in microbial particle-collector grain interactions, the incorporation of a normal distribution in k still results in exponentially declining concentration profiles which are nearly identical to the case with uniform k. This is attributed to the symmetrical nature of the distribution function. The calculations based on the other three distribution functions (eqs 18−20) demonstrate how the inclusion of an asymmetrically distributed deposition rate coefficient results in a nonexponential particle concentration profile (curves c−e).

Incorporation of various distribution functions of k gives rise to considerably different microbial deposition patterns, $S(x)$. It is clearly observed that each distribution function results in a characteristic particle retention profile. A normal distribution in k yields an exponentially decaying microbial deposition pattern. Under most realistic conditions, a log-normal distribution will result in a slightly concave concentration profile. A typical bimodal distribution in k results in a retained particle concentration profile with two distinct regions: an initial steep slope where the "stickier" portion of the particle population is removed rapidly from the pore

TABLE 3. Parameters Used in Probability Distribution Functions

distribution function		parameters	
normal (Gaussian)[a]	$\bar{k} = 1.64 \times 10^{-3}\ s^{-1}$	$\sigma = 4.1 \times 10^{-4}\ s^{-1}$	
log-normal	$\bar{k} = 1.64 \times 10^{-3}\ s^{-1}$ ($\tilde{k} = -6.86$)	$\tilde{\sigma} = 0.94$	
bimodal[b]	$\bar{k}_{low} = 1.64 \times 10^{-4}\ s^{-1}$	$\sigma_{low} = 4.1 \times 10^{-5}\ s^{-1}$	$f_{low} = 0.80$
	$\bar{k}_{high} = 1.48 \times 10^{-2}\ s^{-1}$	$\sigma_{high} = 3.7 \times 10^{-3}\ s^{-1}$	$f_{high} = 0.20$
power-law[c]	$k_{min} = 0\ s^{-1}$	$b = 0.80$	
	$k_{max} = 1.64 \times 10^{-2}\ s^{-1}$		

[a] The mean deposition rate coefficient, $\bar{k}$, is calculated as outlined in Table 1. The standard deviation, σ, is calculated assuming a coefficient of variation (*CV*) of 0.25, where $CV = \sigma/\bar{k}$. [b] $\bar{k}_{low}$ and $\bar{k}_{high}$ are calculated using the parameters in Table 1 and eq 3, where $\alpha_{low} = 0.01$ and $\alpha_{high} = 0.90$ (values similar to those previously estimated from experimental data (*14*)). The standard deviations, σ_{low} and σ_{high}, are calculated assuming $CV_{high} = CV_{low} = 0.25$. [c] The maximum deposition rate coefficient, k_{max}, is set to the theoretical deposition rate coefficient based on transport-limited filtration (i.e., $\alpha = 1$). The constant *A* has a value of 0.455 $s^{0.2}$ and is calculated by substituting eq 20 into eq 15 and solving, subject to the boundary condition $C(0,t) = C_0$.

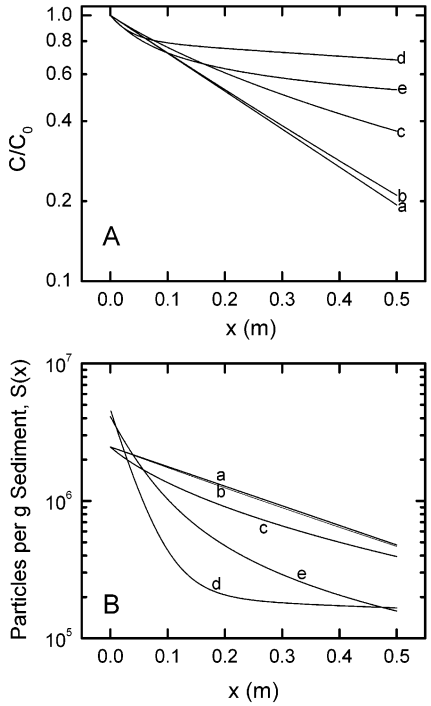

FIGURE 2. Semilog plots of (A) normalized suspended particle concentration and (B) retained particle concentration (number of deposited particles per gram of collector grains), as a function of distance *x* for constant and distributed deposition rate coefficients, *k*. The curves are for (a) constant deposition rate coefficient, (b) normal (Gaussian) distribution in *k*, (c) log-normal distribution in *k*, (d) bimodal distribution in *k*, and (e) power-law distribution in *k*. Parameters used in the calculations are summarized in Tables 1 and 3.

fluid, followed by a shallower slope as the less "sticky" portion of the particle population is removed. The characteristic profile associated to the power-law distribution can be easily identified in a log–log plot as a straight-line. These differences in the shape of the particle retention profiles may go unnoticed for short filtration lengths but become increasingly evident for longer travel distances as demonstrated for a discrete bimodal distribution by Bolster et al. (*13*, *18*). Although each distribution function, $p(k)$, can be generally associated to a distinctive microbial deposition profile, the shape of each profile is also dependent on the values of the model parameters and thus susceptible to variation.

A comparison of the suspended particle profiles (Figure 2a) to the retained particle profiles (Figure 2b) also suggests that the heterogeneity in the deposition rate coefficient is reflected much more strongly in the latter. For instance, at a distance of ca. 10 cm, the fluid-phase concentrations calculated using the different distributions are quite similar ($C/C_0 \approx 0.7$). However, over the same travel distance, the retained microbial particle profiles show marked differences. The results clearly indicate that the profile of retained particles is a more sensitive measure of the variability in the deposition rate due to heterogeneity effects compared to the profile of suspended particles.

It is further noted that the three asymmetric distributions of *k* (curves c–e) result in higher fluid phase particle concentrations (or lower retained concentrations) along most of the column length. At a distance of 10 cm, the fluid-phase particle concentrations (curves a–e) differ by no more than 10%. However, at the column outlet ($x = 50$ cm), the breakthrough concentrations vary by as much as 3.5-fold from the predictions based on a constant *k*. This illustrates how predictions of microbial transport based on a single *k* value (i.e., constant α) may significantly underestimate travel distances. Furthermore, our results imply that accurate predictions of microbial transport in subsurface environments can be significantly enhanced by proper identification of the inherent heterogeneity in the microbial particle–sediment grain interactions and the resulting distribution in the deposition rate coefficient.

Comparison of Experimental Data to Model Predictions. Redman et al. (*10*, *11*) conducted filtration experiments using recombinant Norwalk virus (rNV) particles in a packed bed of highly cleaned quartz grains. The key experimental conditions in this investigation are summarized in Table 2. Their results for two different influent concentrations of virus particles, C_0 (6.5×10^{10} and 1.6×10^9 cm^{-3}) are plotted in Figure 3. Also shown in the figure are model predictions for the deposited virus concentrations based on a power-law distribution of the deposition rate coefficient. The model parameters *b*, k_{min}, and k_{max} were obtained by optimizing the coefficient of determination R^2 (0.99 and 0.95 for the high and low C_0 experiments, respectively). The model predictions suggest that the observed nonexponential deposition behavior of rNV particles is attributed to natural variability in the interactions between the virus particles and the quartz grains, most likely due to inherent heterogeneity in the virus particles, which results in a broad range (i.e., a power-law distribution) of virus deposition rates.

Baygents et al. (*14*) carried out similar column experiments with a Gram-negative bacterial strain designated A1264 in a packed bed of borosilicate glass beads (details are given in Table 2). The profile of retained microbial particles is depicted in Figure 4. Here, the experimental data were modeled with both a power-law and log-normally distributed deposition rate coefficient, with R^2 values of 0.99 and 0.85, respectively. For the log-normal distribution, the two model parameters are the mean ($\tilde{k}$) and the standard deviation ($\tilde{\sigma}$) of the log-normally distributed deposition rate coefficient. Baygents et al. (*14*) fitted their data to a three parameter discrete bimodal distribution (R^2 of 0.99) and a two parameter Weibull distribution (R^2 of 0.84). Although experimental data indicated

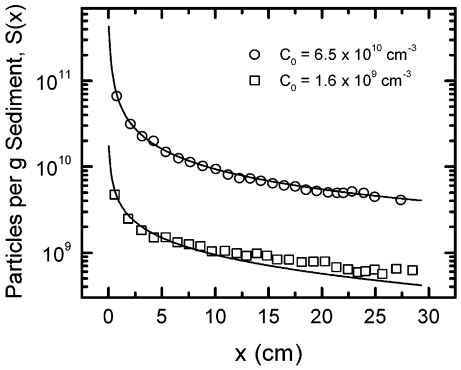

FIGURE 3. Comparison of experimental retained rNV virus particle profiles (symbols) and model predictions (solid lines) using a power-law distribution in k for two influent concentrations: (i) $C_0 = 6.5 \times 10^{10}$ cm^{-3} (optimized model parameters, $b = 1.2$, $k_{min} = 1 \times 10^{-6}$ s^{-1}, $k_{max} = 0.67$ s^{-1}) and (ii) $C_0 = 1.6 \times 10^9$ cm^{-3} (optimized model parameters, $b = 1.5$, $k_{min} = 4 \times 10^{-4}$ s^{-1}, $k_{max} = 0.67$ s^{-1}). Experimental data taken from ref *10*. In addition to the relevant experimental parameters described in Table 2, other useful experimental parameters were virus diameter 38 nm, sand grain diameter 0.22 mm, and approach velocity 0.025 cm/s.

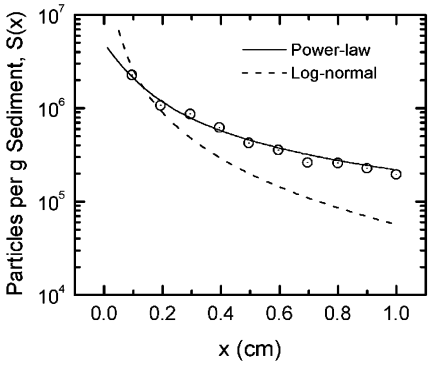

FIGURE 4. Comparison of experimental retained bacterial (A1264) profiles (symbols) and model predictions for two different distributions in k: (i) power-law (optimized model parameters, $b = 0.94$, $k_{min} = 1 \times 10^{-7}$ s^{-1}, $k_{max} = 6.6$ s^{-1}) and (ii) log-normal (optimized model parameters, $\bar{k} = 3.5$, $\tilde{\sigma} = 2.2$). Experimental data taken from ref *14*. In addition to the relevant experimental parameters described in Table 2, other useful experimental parameters were bacterial cell average diameter 0.80 μm, glass bead diameter 40 μm, and approach velocity 0.13 cm/s.

that the bacterial cells exhibited a bimodal distribution in electrophoretic mobility, the fractional size of each subpopulation was not represented in their optimized model parameters.

We have also analyzed other microbial deposition patterns from experiments involving various bacterial strains, sediment (collector) grains, approach velocities, and solution chemistries. As shown in Table 2 (rightmost column), the nonexponential behavior for most of these microbial retention profiles could be well described by a power-law distribution of the deposition rate coefficient. The good fit to a power-law distribution displayed in Figures 3 and 4 above, and the data in Table 2, again supports our suggestion that the nonexponential microbial deposition patterns may be due to a broad range of microbial deposition rates.

Particle Deposition Dynamics (Blocking). Another possible source for nonexponential distribution of deposited microbial particles with travel distance is the phenomenon of blocking. To appropriately describe the dynamic aspects of particle deposition, the transport equation is expressed in terms of particle number concentration rather than mass concentration (*34*):

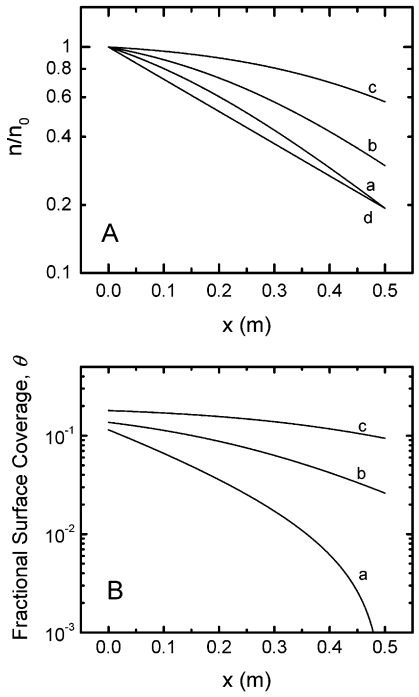

FIGURE 5. Comparison of (A) normalized suspended particle concentrations and (B) fractional surface coverage as a function of distance x for three different times corresponding to 1, 2, and 4 pore volumes (PVs). Note that data are presented in a semilog format. The curves are for (a) Langmuirian blocking function, 1 PV, (b) Langmuirian blocking function, 2 PVs, (c) Langmuirian blocking function, 4 PVs, and (d) classical filtration model (first-order deposition). Note that because the classical filtration model is for "clean-bed" removal (i.e., no blocking), the fractional surface coverage versus x curve for this case in (B) is not applicable. Parameters used in the calculations are summarized in Table 1, with the exception of the column length being 50 cm and the influent particle concentration 4×10^9 cm^{-3}.

$$\frac{\partial n}{\partial t} = D\frac{\partial^2 n}{\partial x^2} - v\frac{\partial n}{\partial x} - \frac{f}{\pi a_p{}^2}\frac{\partial \theta}{\partial t} \tag{21}$$

Here, n is the particle number concentration, θ is the fractional surface coverage of collector grains, defined as the total cross-sectional area of deposited particles per interstitial surface area of the porous medium solid matrix, f is the specific surface area (i.e., interstitial surface area per porous medium pore volume), and a_p is the radius of colloidal particles. When solution and surface conditions limit particle deposition onto collector surfaces to monolayer coverage, the following rate equation is used to describe particle deposition dynamics (*34*)

$$\frac{\partial \theta}{\partial t} = \pi a_p{}^2 k_{dep} B(\theta) n \tag{22}$$

where k_{dep} is the particle transfer rate coefficient and $B(\theta)$ is the dynamic blocking function. The particle transfer rate coefficient is related to the single collector efficiency η by (*35*−*37*)

$$k_{dep} = \frac{\eta \epsilon v}{4} \tag{23}$$

Note that k_{dep} is related to k (previously defined in eq 3) by $k_{dep} = k/f$.

The dynamic blocking function $B(\theta)$ characterizes the transient nature of the particle deposition rate. For simplicity we will use the Langmuirian dynamic blocking function, as

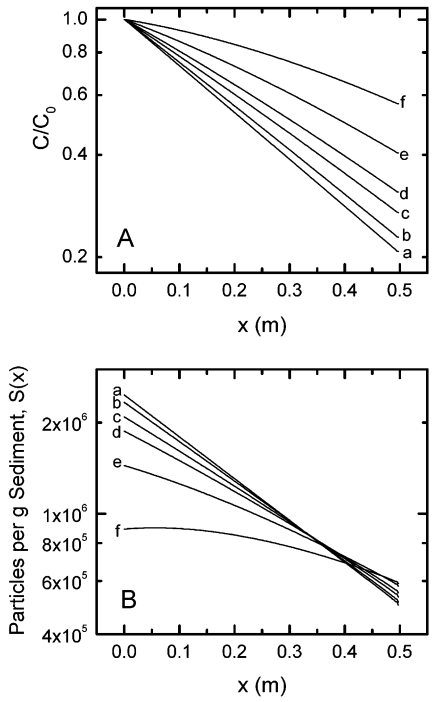

FIGURE 6. Semilog plots of (A) normalized suspended particle concentration and (B) retained particle concentration (number of deposited particles per gram of collector grains), as a function of distance *x* for different values of the release rate coefficient, k_r (expressed as a fraction of the deposition rate coefficient, *k*). The curves are for (a) $k_r = 0$, (b) $k_r = 0.01k$, (c) $k_r = 0.03k$, (d) $k_r = 0.05k$, (e) $k_r = 0.1k$, and (f) $k_r = 0.2k$. Parameters used in the calculations are summarized in Table 1. Note that $S(x)$ is calculated at $t > t_0$ (i.e. 6000 s) to account for deposition occurring during the transient, elution portion of the particle breakthrough curve.

described by Johnson et al. (*34*), to examine the effect of deposition dynamics (blocking) on microbial particle deposition patterns. When this linear blocking function is incorporated into eq 22 for $B(\theta)$, an analytical solution is available for the case where hydrodynamic dispersion effects are neglected (*34*)

$$n(x,t) = \frac{n_0 \exp[k_{dep}\pi a_p^2 \beta n_0 (t - x/v)]}{\exp[k_{dep}\pi a_p^2 \beta n_0 (t - x/v)] + \exp[k_{dep} f x/v] - 1} \quad (24)$$

where β is the excluded area parameter, equivalent to the reciprocal of the maximum attainable surface coverage, θ_{max}.

The particle concentration profiles calculated using both the classical filtration model (first-order deposition) and eq 24 (note when blocking occurs deposition follows second-order kinetics) are compared in Figure 5a,b in semilog format. The curves for blocking were generated using a β value of 5 (i.e., $\theta_{max} = 0.2$) (*34*) for three different lengths of particle injection corresponding to 1, 2, and 4 pore volumes. All other parameters used in the calculations are shown in Table 1, with the exception of the column length being 50 cm and the influent particle concentration 4×10^9 cm^{-3}. Similar to the results obtained in the previous section when an asymmetric distribution of deposition rate coefficient was considered, the inclusion of blocking results in higher solution phase microbial particle concentrations along the length of the column. Furthermore, when blocking dynamics are considered, the profiles of solution phase microbial particles and fractional surface coverage (retained particles) decay in a nonexponential fashion and are convex in shape. In contrast, inspection of the retained particle profiles when asymmetric distributions of *k* are considered (Figure 2b) reveals that these curves are concave in shape. Thus, our results underscore the importance of the retained particle profiles in identifying the key mechanisms controlling the deposition behavior of microbial particles in porous media.

Microbial Particle Release. The theoretical analysis of microbial particle deposition presented earlier assumed the particles to deposit irreversibly onto collector grains. Several studies involving transport of microbial pathogens suggest that deposition and release occur simultaneously (*38*, *39*) with the microbial release rate being much smaller than the deposition rate. Thus, release of deposited microbial particles may also result in deviations from classical colloid filtration theory.

To analyze microbial particle release, we solve eq 1 coupled with

$$\frac{\rho_b}{\epsilon}\frac{\partial S}{\partial t} = kC - \frac{\rho_b}{\epsilon} k_r S \quad (25)$$

where k_r is the particle release rate coefficient. Lapidus and Amundson (*40*) presented an analytical solution to eqs 1 and 25 for the case when the initial particle concentration in the column is set to zero, the particle concentration at the column inlet boundary is given as a constant C_0, and the dispersive particle flux is set to zero at the column outlet boundary (as in eq 7)

$$\frac{C}{C_0} = \exp\left(\frac{vx}{2D}\right)[F(t) + k_r \int_0^t F(\tau)\, d\tau] \quad (26)$$

where

$$F(t) = \exp(-k_r t)\int_0^t I_0[2\sqrt{k k_r \tau (t-\tau)}]\frac{x}{2\sqrt{\pi D \tau^3}} \times \exp\left(-\frac{x^2}{4D\tau} - \tau d\right) d\tau \quad (27)$$

and

$$d = \frac{v^2}{4D} + k - k_r \quad (28)$$

Concentration profiles of suspended and retained particles calculated using eqs 26−28 for different values of the particle release rate coefficient (k_r) are presented in Figure 6 (parts a and b, respectively). The parameters used in these calculations are summarized in Table 1, with the exception that the column length has been extended to 50 cm and the time of injection, t_0, has been increased to 5000 s. Here, the values of k_r are presented as a fraction of the deposition rate coefficient, *k*. For the case where $k_r = 0$ (i.e., neglecting particle release), the results are identical to those obtained previously using the classical filtration model (i.e., curve a in Figure 2a,b). As the value of the release rate coefficient is increased, we note that the particle concentration profiles deviate from those predicted by filtration theory. Thus, the incorporation of particle release results in higher fluid-phase microbial particle concentrations along the length of the column, as noted previously when heterogeneity or blocking effects were considered. Although the microbial particle concentration profiles do not follow classical filtration theory, the profiles calculated using release rate coefficients $k_r < 0.1k$ are still exponential. Thus, for most realistic conditions, the release of deposited microbial particles cannot account for the nonexponential microbial deposition behavior observed in column experiments. Only for sufficiently large and perhaps unrealistic release rate coefficients ($k_r > 0.1\,k$), the suspended and retained particle concentration profiles exhibit nonexponential behavior. Furthermore, similar to the results

obtained in the previous section when the effects of blocking were described, the inclusion of large microbial release rates results in convex retained particle profiles.

Acknowledgments

The authors acknowledge the support of the U.S. EPA (Award R-82901001-0), the National Science Foundation (Grant CHE-0089156), the Natural Sciences and Engineering Research Council of Canada (NSERC) for a graduate student fellowship to N.T., and the Yale Institute for Biospheric Studies (YIBS) for a postdoctoral fellowship to J.A.R.

Literature Cited

(1) Thomas, J. M.; Ward, C. H. *Environ. Sci. Technol.* **1989**, *23*, 760−766.
(2) Tufenkji, N.; Ryan, J. N.; Elimelech, M. *Environ. Sci. Technol.* **2002**, *36*, 422A−428A.
(3) Gerba, C. P.; Powelson, D. K.; Yahya, M. T.; Wilson, L. G.; Amy, G. L. *Water Sci. Technol.* **1991**, *24*, 95−102.
(4) Schijven, J. F.; Hassanizadeh, S. M. *Crit. Rev. Environ. Sci. Technol.* **2000**, *30*, 49−127.
(5) Redman, J. A.; Grant, S. B.; Olson, T. M.; Hardy, M. E.; Estes, M. K. *Environ. Sci. Technol.* **1997**, *31*, 3378−3383.
(6) Camesano, T. A.; Logan, B. E. *Environ. Sci. Technol.* **1998**, *32*, 1699−1708.
(7) Yao, K. M.; Habibian, M. T.; O'Melia, C. R. *Environ. Sci. Technol.* **1971**, *5*, 1105−1112.
(8) Jewett, D. G.; Hilbert, T. A.; Logan, B. E.; Arnold, R. G.; Bales, R. C. *Water Res.* **1995**, *29*, 1673−1680.
(9) Harter, T.; Wagner, S.; Atwill, E. R. *Environ. Sci. Technol.* **2000**, *34*, 62−70.
(10) Redman, J. A.; Estes, M. K.; Grant, S. B. *Colloid Surf. A, Physicochem. Eng. Asp.* **2001**, *191*, 57−70.
(11) Redman, J. A.; Grant, S. B.; Olson, T. M.; Estes, M. K. *Environ. Sci. Technol.* **2001**, *35*, 1798−1805.
(12) Albinger, O.; Biesemeyer, B. K.; Arnold, R. G.; Logan, B. E. *FEMS Microbiol. Lett.* **1994**, *124*, 321−326.
(13) Bolster, C. H.; Mills, A. L.; Hornberger, G. M.; Herman, J. S. *Water Resour. Res.* **1999**, *35*, 1797−1807.
(14) Baygents, J. C.; Glynn, J. R.; Albinger, O.; Biesemeyer, B. K.; Ogden, K. L.; Arnold, R. G. *Environ. Sci. Technol.* **1998**, *32*, 1596−1603.
(15) Martin, M. J.; Logan, B. E.; Johnson, W. P.; Jewett, D. G.; Arnold, R. G. *J. Environ. Eng.* **1996**, *122*, 407−415.
(16) Simoni, S. F.; Harms, H.; Bosma, T. N. P.; Zehnder, A. J. B. *Environ. Sci. Technol.* **1998**, *32*, 2100−2105.
(17) Silliman, S. E.; Dunlap, R.; Fletcher, M.; Schneegurt, M. A. *Water Resour. Res.* **2001**, *37*, 2699−2707.
(18) Bolster, C. H.; Mills, A. L.; Hornberger, G.; Herman, J. *Ground Water* **2000**, *38*, 370−375.
(19) Kretzschmar, R.; Barmettler, K.; Grolimund, D.; Yan, Y. D.; Borkovec, M.; Sticher, H. *Water Resour. Res.* **1997**, *33*, 1129−1137.
(20) Grolimund, D.; Elimelech, M.; Borkovec, M.; Barmettler, K.; Kretzschmar, R.; Sticher, H. *Environ. Sci. Technol.* **1998**, *32*, 3562−3569.
(21) Martin, R. E.; Bouwer, E. J.; Hanna, L. M. *Environ. Sci. Technol.* **1992**, *26*, 1053−1058.
(22) Harvey, R. W.; Garabedian, S. P. *Environ. Sci. Technol.* **1991**, *25*, 178−185.
(23) Iwasaki, T. *J. Am. Water Work Assoc.* **1937**, *29*, 1591.
(24) van Genuchten, M. T.; Alves, W. J. *Analytical Solutions of the One-Dimensional Convective-Dispersive Solute Transport Equation*; U.S. Department of Agriculture, Agricultural Research Service: Washington, D.C, 1982.
(25) Jury, W. A.; Roth, K. *Transfer Functions and Solute Movement Through Soils: Theory and Applications*; Birkhauser Verlag: Basel, Switzerland, 1990.
(26) de Marsily, G. *Quantitative Hydrogeology: Groundwater Hydrology for Engineers*; Academic Press: Orlando, 1986.
(27) Dong, H. *J. Microbiol. Methods* **2002**, *51*, 83−93.
(28) Camesano, T. A.; Abu-Lail, N. I. *Biomacromolecules* **2002**, *3*, 661−667.
(29) Elimelech, M.; Gregory, J.; Jia, X.; Williams, R. A. *Particle Deposition & Aggregation: Measurement, Modelling, and Simulation*; Butterworth-Heinemann: Oxford, England, 1995.
(30) Aitchison, J.; Brown, J. A. C. *The Log-normal Distribution*; Cambridge University Press: London, 1963.
(31) Derjaguin, B. V.; Landau, L. D. *Acta Physicochim. U.S.S.R.* **1941**, *14*, 733−762.
(32) Verwey, E. J. W.; Overbeek, J. T. G. *Theory of the Stability of Lyophobic Colloids*; Elsevier: New York, NY, 1948.
(33) Elimelech, M. *Water Res.* **1992**, *26*, 1−8.
(34) Johnson, P. R.; Elimelech, M. *Langmuir* **1995**, *11*, 801−812.
(35) Song, L.; Elimelech, M. *Colloid Surf. A, Physicochem. Eng. Asp.* **1993**, *73*, 49−63.
(36) Tien, C. *Granular Filtration of Aerosols and Hydrosols*; Butterworth: Stoneham, MA, 1989.
(37) Prieve, D. C.; Ruckenstein, E. *AIChE J.* **1974**, *20*, 1178−1187.
(38) Johnson, W. P.; Zhang, P.; Gardner, P. M.; Fuller, M. E.; DeFlaun, M. F. *Appl. Environ. Microbiol.* **2001**, *67*, 4908−4913.
(39) Meinders, J. M.; van der Mei, H. C.; Busscher, H. J. *J. Colloid Interface Sci.* **1995**, *176*, 329−341.
(40) Lapidus, L.; Amundson, N. R. *J. Phys. Chem.* **1952**, *56*, 984−988.
(41) Li, Q. M.S. Thesis, The University of Arizona, 1996.

Received for review June 12, 2002. Revised manuscript received November 13, 2002. Accepted November 26, 2002.

ES025871I